Effect of mass ratio in common envelope flows

Soumi De,[1,2] Tassos Fragos,[3,2] Morgan Macleod,[4,5,2] Ilya Mandel,[6,2] and Enrico Ramirez-Ruiz[7,2]

[1] *Syracuse University, Syracuse, NY 13244, USA*
[2] *DARK, Niels Bohr Institute, University of Copenhagen, Blegdamsvej 17, 2100 Copenhagen, Denmark*
[3] *Geneva Observatory, University of Geneva, Chemin des Maill ettes 51, 1290 Sauverny, Switzerland*
[4] *School of Natural Sciences, Institute for Advanced Study, 1 Einstein Drive, Princeton, New Jersey 08540, USA*
[5] *Harvard Smithsonian Center for Astrophysics, Cambridge, MA, USA*
[6] *School of Physics and Astronomy, University of Birmingham, Edgbaston, Birmingham B15 2TT, United Kingdom*
[7] *Department of Astronomy and Astrophysics, University of California, Santa Cruz, CA 95064*

In this paper we study the flows of material around the secondary star in binaries evolving within a common envelope. We establish that gravitational focusing in common envelope flows is governed by the size of the orbit of the binary system. We perform numerical experiments using the Wind Tunnel formalism over the space of our parameters which comprises of the mass ratio of the binary system, and flow parameters like "Mach number" and gradient of density. We then compute the accretion and drag force coefficients associated with the flows. We also illustrate the inspiral evolution of the stars in a binary evolving inside a common envelope, and show how a greater mass ratio leading to a greater drag force in the flow would tighten the orbit.

I. INTRODUCTION

A common envelope phase is a short-lived phase in the lives of binaries in which the two stars evolve inside a single common envelope. It occurs when one of the stars in the binary grows out of its main sequence phase onto a giant branch. The primary star then impinges upon the orbit of the secondary star and engulfs it. The two stars then interact with each other via mass transfer which takes place from the primary to the secondary. This sets the beginning of the phase of common envelope evolution in the system. The common envelope phase can be significant in determining the fate of the stars in the system. It is important to understand this phase in order to understand the formation of gravitational wave sources and cosmological standard sirens.

II. GRAVITATIONAL FOCUSING

Following from the Bondi Hoyle Lyttleton theory of accretion, [1] we consider a test particle flowing in the material surrounding the embedded secondary star in the envelope, and examine its behavior in the presence of the secondary star. The test particle will experience a force of attraction due to the secondary star's gravity, which causes it to move towards the star and get focused behind it. However, there is a condition as to whether the particle will be accreted on the embedded star. That is determined by the total energy of the particle, given by :

$$\frac{1}{2}v_\infty^2 - \frac{GM_{acc}}{r} < 0 \tag{1}$$

where v_∞ is the relative velocity of the embedded star to the gas flowing past it, M_{acc} is the mass of the embedded star which is the accretor, and r is the radial distance of the test particle to the embedded star. v_∞ should also take into account the speed of sound. However, in our studies we consider flows that are supersonic, ie. velocity of the material is greater than the speed of sound. A negative total energy would imply that the particle is energetically bound to the star. This leads us to determining a characteristic cross section inside which material will be accreted. The radius of that cross-section is the accretion radius - R_a. R_a can be expressed as :

$$R_a = \frac{2GM_{acc}}{v_\infty^2} \tag{2}$$

This will eventually lead to determining a mass and momentum flux that will be accreted onto the star. Fig. 1 is a pictorial representation of a point particle being accreted onto the star. Although one would expect the

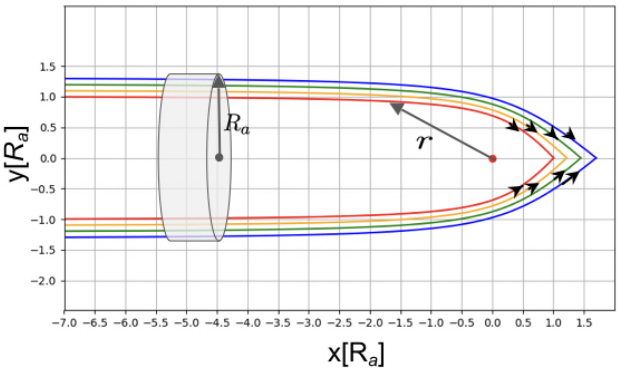

FIG. 1. Illustration of a point test particle in the gas being gravitationally focused behind the embedded secondary star. The embedded secondary star is denoted by the red dot, and the arrow-lines represent the flow of streamlines.

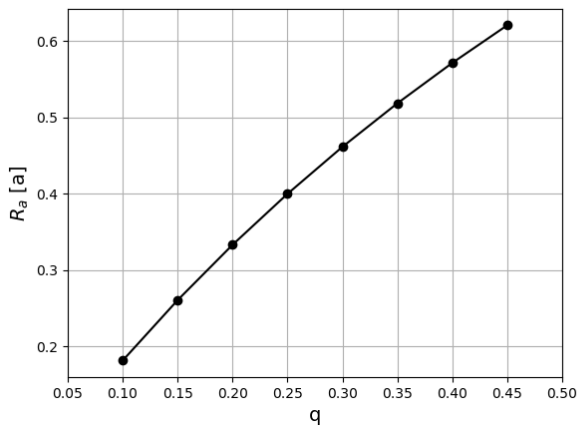

FIG. 2. Variation of accretion radius expressed in terms of the size of the orbit of a binary $R_a[a]$ with mass ratio, q - calculated analytically.

trajectories of flows of the material to look as represented in the figure, pressure effects in the gas will modify the trajectories and the streamlines will not be as focused as shown in the diagram. At the point where the streamlines are focused, the momentum of the flow is canceled due to the symmetry of the streamlines. The gas that is focused is then drawn in to the embedded star, in a direction which would be opposite to the direction of the material flowing in. [2] [3]

The keplerian orbital velocity of the secondary object around the primary object is given by:

$$v_k = \Big(\frac{GM}{a}\Big)^{1/2} \tag{3}$$

where $M = M_1 + M_2$ is the total mass of the binary. The relative velocity of the secondary to the envelope gas, v_∞ is related to the keplerian velocity of the secondary, v_k as :

$$v_\infty = f_k v_k \tag{4}$$

Thus, f_k is the fraction of the keplerian velocity that contributes to the relative velocity. In our studies that we present in this paper, we have considered a simplified scenario, where $f_k = 1$.

From the energy conditions for accretion and the conditions for the orbital motion of the secondary around the primary, the accretion radius, R_a can be expressed in terms of the orbital radius, a which in turn is defined by the mass ratio, $q = M_2/M_1$, where M_2 is the smaller star and M_1 is the bigger star in the binary. [2].

$$\frac{R_a}{a} = \frac{2}{f_k^2}\frac{M_2}{M} = \frac{2}{f_k^2}\frac{1}{1+q^{-1}} \tag{5}$$

For a given value of q, one can calculate R_a in terms of a. The variation of R_a in terms of a with q is shown in Fig2. It can be seen that as q increases, $R_a[a]$ also increases. Since R_a describes the size of the accretion structure, and a is the size of the orbit of the secondary around the primary, $R_a[a]$ denotes the fraction of the orbit that is involved in the accretion. As $q \to 1$ in a common envelope scenario, $R_a \to a$. This directs us to establishing the idea that the gravitational focusing in common envelope flows is governed by the size of the orbit.

III. SETUP FOR NUMERICAL EXPERIMENTS

Our work is built on the basics of the formalism of studying common envelope flows develped in [4] and [2]. The numerical experiments that we perform use the common envelope envelope wind tunnel setup. The wind tunnel setup in a three dimensional hydrodynamical setup, and we use the FLASH code [5] to solve the equations of hydrodynamics. Our computational domain is considered to be a three dimensional cartesian domain, and therefore we study the flows in the very locality of the secondary star, maintaining the validity of cartesian coordinates within the domain. We made sure that no significant errors are introduced for not taking into account the curvature of the star. The embedded secondary object is considered to be a point mass that is placed at the origin of the box, which is our computational domain. The sink boundary condition has been defined to be $R_s = 0.05R_a$.

The winds representing the flow of material in the envelope enter into the box from the $-X$ boundary and gets accreted onto the embedded star. The embedded star is considered as a sink into which material flows in. The wind tunnel setup also assumes a diode boundary condition condition at the $+x$, $+y$, and $\pm z$ boundaries, according to which material can leave but not re-enter into the grid. The winds have a gradient of pressure and density in the y direction. We also consider the winds to be in hydrostatic equilibrium with the primary star's gravity in the y direction. The size of the box inside which we perform our computations is considered to be smaller than the size of the orbit, a, as we study the flows of the material in the locality of the secondary object only. At the same time the box size is taken to be greater than the accretion radius, R_a, as we want to take into account all the characteristics of the flow. In all our numerical experiments, we consider a box size that scales as half the size of the orbit.

The material flowing into the box has a very high velocity. As this velocity exceeds the speed of sound around the secondary object, it creates a very large pressure difference, which is called a shock wave. The shock wave then propagates backwards and outwards from the embedded secondary object in the form of a bow. Material on crossing the shock wave, decreases in velocity and increases in pressure and density. This supersonic flow of material around the secondary object is quantified by

the "Mach number" $\mathcal{M} = v/c_s$, which should be greater than 1 in this scenario. Thus the "Mach number" sets the criteria for the shock wave. Higher the value of $\mathcal{M}$, stronger is the shock wave. It was shown in [2] that the "Mach number" depends on the density gradient across the accretion radius, ϵ_ρ as follows :

$$\mathcal{M}^2 = \epsilon_\rho \frac{(1+q)^2}{2q} f_k^4 \Big(\frac{\Gamma_s}{\gamma_1}\Big)^{-1} \tag{6}$$

where Γ_s is the polytropic index of the stellar profile, and γ_1 determines the gas envelope's response to compression. For a fully convective envelope, $\Gamma_s \approx \gamma_1$, whereas for a radiative envelope $\Gamma_s < \gamma_1$. The density gradient across the accretion radius is expressed as [4] [2]:

$$\epsilon_\rho = \frac{Ra}{H_\rho} \tag{7}$$

where $H_\rho = -\rho dr/d\rho$ is the density scale height. As ϵ_ρ increases, the "Mach number" increases. Towards the outer regions of the star, radiative losses cause a reduction in scale height, leading to a steeper density gradient to occur in that region.

IV. RESULTS

A. Flows in the numerical experiments

We have performed wind tunnel numerical experiments for "Mach numbers" 1.15, 1.39, 1.7, 2.2, 2.84, 3.48, and 5.0, for values of mass ratio 1/10, 1/7, 1/5, 1/4, 1/3, for common envelope structures which can be described by a $(\Gamma_s, \gamma_1 = 5/3)$=(5/3, 5/3) adiabatic equation of state. As Γ_s equals γ_1, we consider fully convective envelopes. An envelope having a $\gamma = 5/3$ equation of state would occur for relatively smaller massive stars $1 - 8M_\odot$, whereas a $\gamma = 4/3$ equation of state would occur for more massive stars of $30 - 40M_\odot$. Fig 3 shows snapshots from the numerical experiments performed for mass ratio 1/10 and 1/3, and Mach numbers 1.39, 2.2, and 3.48. The images show the orbital plane of the binary with the black dot towards the representing the embedded secondary star. Moving up in the y-axis implies moving towards the outer regions of the star. Material can be seen to be flowing in from the $-X$ boundary, and be accreted onto the embedded secondary star. The white lines with arrowheads represent the velocity streamlines of the flow. The colorbar denotes a variation of density in the flow of the material. The bow shape in the images represents the primary shock wave, formed as a result of the large pressure difference created due to the supersonic flow of material around the embedded star. As discussed earlier, an increase in the "Mach number" implies an increase in the gradient of density, ϵ_ρ. Also, a high gradient of density occurs towards the outer regions of the star, whereas a low gradient of density occurs towards the inner regions of the star. Thus moving from the images on the right to the images on the left in Fig. 3, the embedded secondary object could be thought as inspiraling from the outer regions of the envelope towards the center.

One of the flow characteristics that can be noticed in the images in Fig. 3 is that the flow symmetry is broken as the gradient of density increases. That happens because the gradient of density prevents the momentum of the streamlines to cancel as predicted in Section 2, thus introducing a net angular momentum to the flow. This causes the accretion of material to be disturbed, and the accretion rate drops.

Comparing the simulations for $q = 1/3$ to $q = 1/10$, it can be seen that the higher mass ratio causes the flows to not be as well focused. This happens because as the mass ratio increases, $R_a[a]$ increases. This implies that the accretion radius then becomes a larger fraction of the orbit size, causing the flows to be focused from a distance that is a larger multiple of the accretion radius, which causes poorer focusing.

B. Mass accretion rate

Fig. 4 shows results from the wind tunnel experiments that we performed, demonstrating the variation of the coefficient of the mass accretion rate with mass ratio, for the different values of "Mach numbers" for which the experiments were performed.

The coefficient of the mass accretion rate is obtained by normalizing the mass accretion rate in the system to the Bondi-Hoyle-Lyttleton theory mass accretion rate.

As the mass ratio increases, the accretion radius becomes a larger fraction of the size of the orbit, as discussed in Section 2., thus causing a large cross section of material to be encountered with, which will be available to be accreted in. This large amount of material which can be accreted in cause an increase in the mass accretion rate.

C. Drag force

The drag force is caused as a result of material accumulating behind the embedded secondary object as a result of gravitational focusing. The mass distribution around the embedded object not being spherically symmetric, causes a net gravitational force directed along the direction of motion of the object, and is called as the drag force. The drag force causes a deceleration in

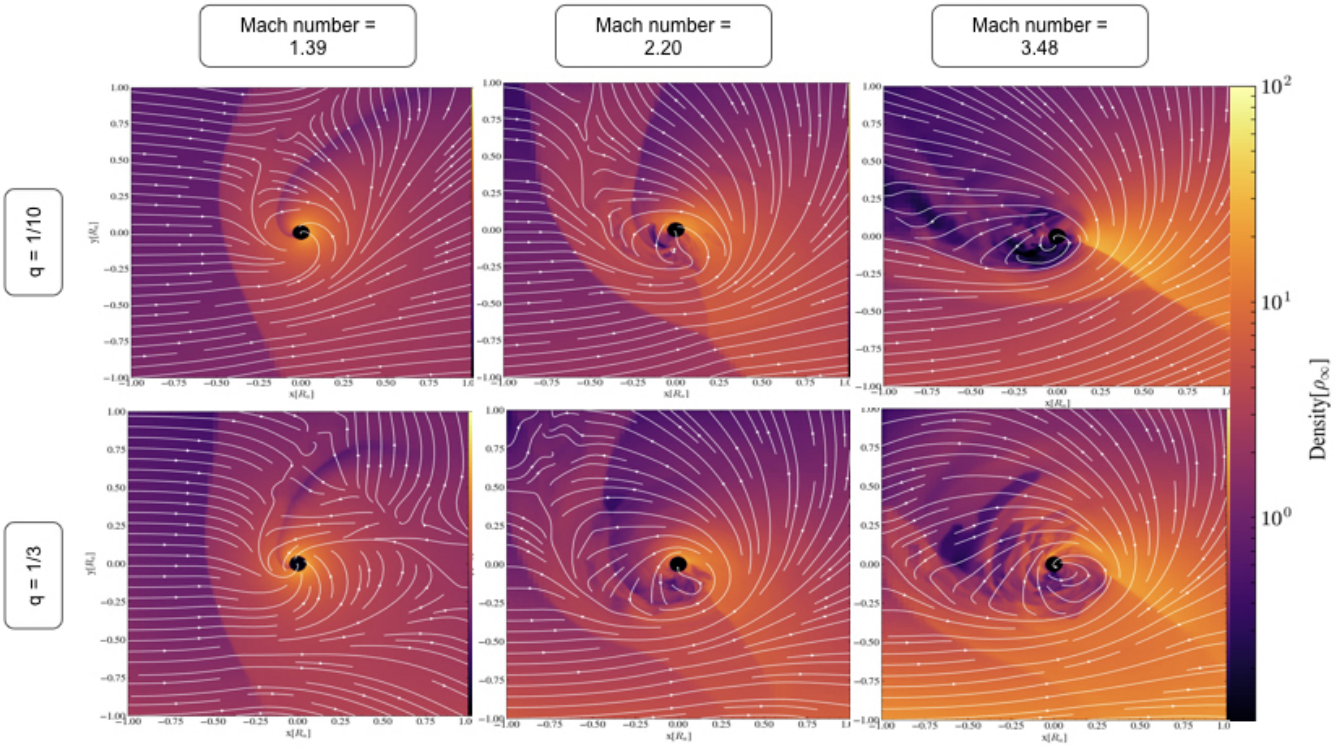

FIG. 3. Snapshots from the wind tunnel experiments performed, showing the the z=0, orbital plane of the binary. The simulations in the upper panels were done with with mass ratio $q = 1/10$, and those in the lower panel were done with $q = 1/3$. The simulations were done with three values of Mach numbers : 1.39, 2.2, and 3.48 (left to right).

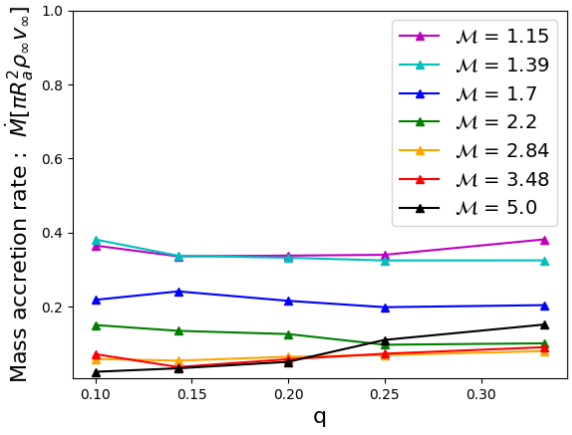

FIG. 4. Results from numerical experiments showing variation of the median mass accretion rate coefficient onto the sink with changing mass ratio, for different values of Mach number.

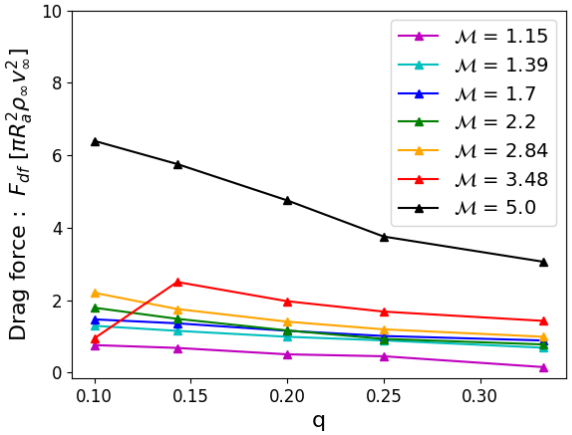

FIG. 5. Results from numerical experiments showing variation of the dynamical friction drag force coefficient with changing mass ratio, for different values of Mach number. The drag forces have been calculated at the outermost radii in the simulations which are $2.75R_a$, $2.0R_a$, $1.5R_a$, $1.25R_a$, and $1.0R_a$ for q=1/10, 1/7, 1/5, 1/4, and 1/3 respectively.

the motion of the secondary embedded object. Fig. 5 includes results from the wind tunnel experiments that we performed, showing the variation of the coefficient of the dynamical friction drag force with mass ratio, for the different values of "Mach numbers" for which the experiments were performed. The coefficient of the drag force is obtained by normalizing the drag force in the system to the Bondi-Hoyle-Lyttleton theory drag force. For each of the experiments, we integrated out the drag force upto the outermost radii of the simulations.

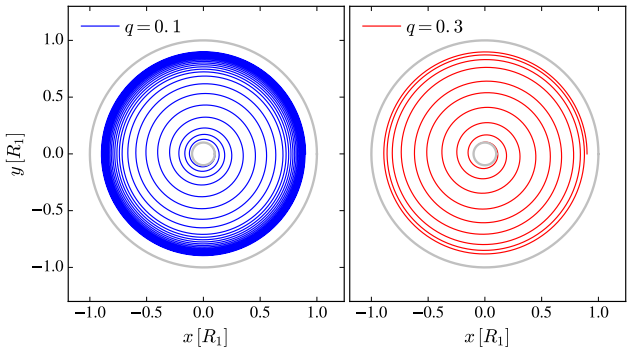

FIG. 6. Illustration of inspiral evolution of stars inside a common envelope. The primary is a [$80M_\odot$, $725R_\odot$] star and the inspiral evolution is demonstrated for two cases where of the companion stars are related to the primary by $q = 1/10$ and $1/3$.

As the mass ratio increases, the drag force also increases. This is because, an increasing mass ratio causes the accretion radius to become a larger fraction of the orbit, as discussed in Section 2. In this scenario, a larger cross section of material can be encountered, and material can be drawn in from deeper within the star. The deeper it is within the star from which the material is drawn in, the denser the material is. The more dense the material that is drawn in is, as compared to the material around the embedded secondary object, the more it contributes to the enhancement of the drag force.

V. ILLUSTRATION OF INSPIRAL EVOLUTION OF STARS IN A COMMON ENVELOPE

Illustrated in Fig. 6 is the inspiral evolution of the stars in a common envelope. The systems demonstrated consist of a [$80M_\odot$, $725R_\odot$] primary star, and the two cases are for the companion secondary stars related to the primary via $q = 1/10$ and $1/3$. The equation of motion of the secondary around the enclosed mass of the primary was integrated, and the drag coefficients from the numerical Wind Tunnel experiments for the $q = 1/10$ and $q = 1/3$ cases were included. The evolution of the secondary around the primary in the envelope was then plotted.

It can be seen, that as the mass ratio increases, the orbit tightens more rapidly. That can be explained in the context of the role of the drag force. An increasing mass ratio would cause an increase in the drag force. An increasing drag force would cause a larger deceleration in the motion of the embedded secondary object, and would cause the orbit to decay out faster. This would lead to explaining the lesser number of orbits that is required for the object to inspiral in.

VI. CONCLUSIONS AND FUTURE WORK

An important and interesting characteristic of common envelope flows that we learnt in this work was that gravitational focusing in these flows is governed by the size of the orbit, that is in turn defined by the mass ratio. Our work would mainly contribute to mapping out the coefficients of accretion and drag force with changing values of the mass ratio. Beyond what is reported in this letter, we would expand our space of parameters in mass ratio and "Mach numbers" to collect more data points for results that would help us understand the flows in the common envelope evolution better. We also intend to investigation to massive star system of larger masses $\approx 30-40M_\odot$, corresponding to $(\Gamma_s, \gamma) = (4/3, 4/3)$, and study the coefficients of accretion and drag corresponding to our grid of parameters.

VII. ACKNOWLEDGEMENTS

We thank the Niels Bohr Institute for its hospitality while part of this work was completed, and acknowledge the Kavli Foundation and the DNRF for supporting the 2017 Kavli Summer Program. The software used in this work was in part developed by the DOE-supported ASCI/Alliance Center for Astrophysical Thermonuclear Flashes at the University of Chicago. Simulation visualizations and analysis were carried out using the yt toolkit [6]. This research made use of astropy, a community developed core Python package for Astronomy (Astropy Collaboration et al. 2013). The numerical simulations and other computation for this research were carried out in the Hyperion cluster at the School of Natural Sciences, Institute for Advanced Study, Princeton, and in the Syracuse University SUGWG cluster.

[1] R. Edgar, New Astronomy Reviews **48**, 843 (2004).
[2] M. MacLeod, A. Antoni, A. Murguia-Berthier, P. Macias, and E. Ramirez-Ruiz, The Astrophysical Journal **838**, 56 (2017).
[3] A. Murguia-Berthier, M. MacLeod, E. Ramirez-Ruiz, A. Antoni, and P. Macias, The Astrophysical Journal **845**, 173 (2017).
[4] M. MacLeod and E. Ramirez-Ruiz, The Astrophysical Journal Letters **798**, L19 (2015).
[5] B. Fryxell, K. Olson, P. Ricker, F. X. Timmes, M. Zingale, D. Q. Lamb, P. MacNeice, R. Rosner, J. W. Truran, and H. Tufo, Astrophysical Journal, Supplement **131**, 273 (2000).
[6] M. J. Turk, B. D. Smith, J. S. Oishi, S. Skory, S. W. Skillman, T. Abel, and M. L. Norman, The Astrophysical Journal Supplement Series **192**, 9 (2011).